Insights into the Application of Metal-Organic Frameworks for Molecular Photovoltaics

13

Matthew C. Kessinger and Amanda J. Morris

This chapter is dedicated to Professor Peter J. Derrick who passed away during the writing of this chapter.

Contents

13.1 Introduction 384
13.2 What Are Metal-Organic Frameworks? 384
13.3 The Advantages of MOFSCs 386
13.4 Potential Considerations of MOFSCs 387
13.5 Fundamental Studies on Charge Separation 388
13.6 Charge Transfer and Redox Hopping 390
13.7 Literature Examples of MOFSCs 393
13.8 Conclusions and Future Outlook 403
References 404

Abstract

Within the area of state-of-the-art photovoltaics, organic photovoltaics, and, more specifically, polymer-based photovoltaics have gained significant interest as novel molecular photovoltaic materials. As a subset of traditional polymers, multi-dimensional metal coordination polymers, known as metal-organic frameworks (MOFs), have shown promise as sensitizers for molecular photovoltaics. These state-of-the-art devices have been termed metal-organic framework solar cells (MOFSCs) and represent an emerging alternative to traditional photovoltaic

Author Contribution

The first draft was written by Matthew Kessinger. The final draft was reviewed and edited by Dr. Amanda J. Morris and Matthew Kessinger.

M. C. Kessinger · A. J. Morris (✉)
Virginia Tech, Blacksburg, VA, USA
e-mail: kessm05@vt.edu; ajmorris@vt.edu

T. A. Atesin et al. (eds.), *Nanostructured Materials for Next-Generation Energy Storage and Conversion*, https://doi.org/10.1007/978-3-662-59594-7_13

materials. In this chapter, an overview of the application of MOFs as a sensitizer for MOFSCs is explored including their advantages and limitations when compared to molecular dyes, the origin of electronic transport in MOF materials, and a selection of the proof-of-concept studies illustrating the feasibility of MOFSCs in bulk applications.

13.1 Introduction

This book chapter will focus on the preparation and use of metal-organic frameworks (MOFs) as a new class of sensitizers for dye-sensitized solar cells (DSSCs). The chapter will begin with a discussion of the fabrication and operational mechanism of DSSCs. Following this, a discussion of MOFs and their characteristic properties will be presented outlining the benefits and considerations for the implementation of metal-organic framework sensitized solar cells (MOFSCs). Finally, the chapter will provide examples and analysis of frameworks used in MOFSCs. Currently, there is only a select handful of MOFSCs in the literature, which primarily provide proof-of-concept experiments on the working principles of MOFSCs. Each of these examples will be discussed in detail to reiterate and demonstrate the current challenges associated with MOFSCs, and the unique solutions researchers are currently investigating to meet these challenges. The chapter will then be concluded with a prospectus on the outlook and challenges of MOFSCs as an emerging class of state-of-the-art molecular photovoltaics.

Before examining the finer details of MOFSCs, it is first useful to discuss their predecessor: the dye-sensitized solar cell (DSSC). Dye-sensitized solar cells are second-generation photovoltaic devices based on the original design of Grätzel. In this cell architecture, the absorption of sunlight by a dye-sensitizer or chromophore leads to the generation of free charge carriers, which then power an external load [31]. The typical device architecture for a DSSC consists of three main components: a working electrode or photoanode, a counter electrode, and a liquid or solid-state electrolyte. The working electrode is composed of a sensitizing chromophore chemisorbed onto a wide bandgap semiconductor, usually titanium dioxide (TiO_2) deposited on a conductive glass substrate such as fluorine-doped tin oxide (FTO). The working electrode is responsible for the absorption of sunlight and ultimately, the generation of a charge-separated state. Opposite the working electrode is the counter electrode. This electrode is typically a platinum-coated conductive glass substrate. The two electrodes are separated by a polymer spacer creating an interelectrode space. This void space is then filled with a redox-active electrolyte, which is responsible for regenerating the chromophore during operation and carrying photogenerated holes to the counter electrode. The general operational mechanism for a DSSC is summarized in Scheme 13.1.

13.2 What Are Metal-Organic Frameworks?

Metal-organic frameworks represent a unique class of coordination polymers in which organic linkers coordinate to metal ions or metal-oxo clusters to form highly ordered and tunable two- or three-dimensional assemblies (Scheme 13.2) [47]. Specifically, MOFs

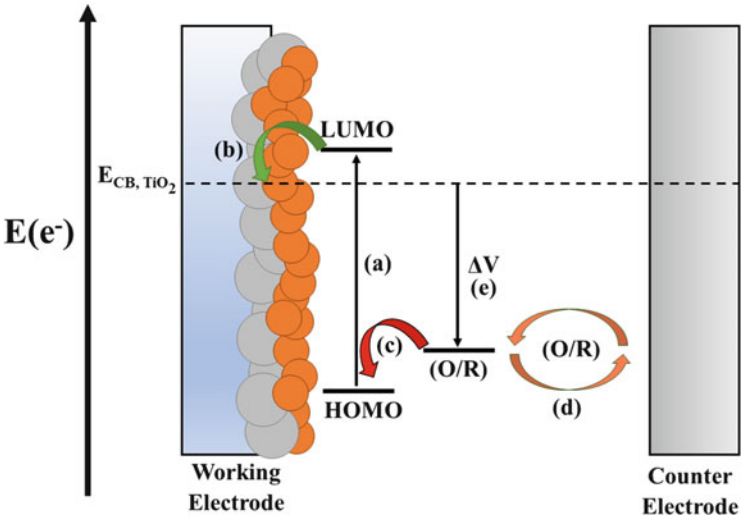

Scheme 13.1 Operational mechanism of a conventional DSSC. (a) Absorption of sunlight by a chromophore promotes an electron from the highest occupied molecular orbital of the dye (HOMO) to its lowest unoccupied molecular orbital (LUMO). (b) Due to the energy differential between the energy of the LUMO of the chromophore and the energy of the conduction band of the TiO_2 (dashed line), the excited electron is injected into the titania (TiO_2) conduction band. (c) The chromophore is then regenerated by electron transfer from a redox couple in the electrolyte. (d, e) The now oxidized redox couple diffuses to the counter electrode where it accepts an electron generating photovoltage

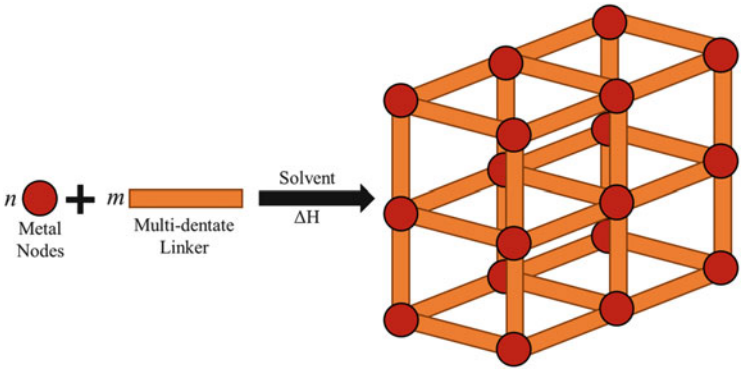

Scheme 13.2 Schematic representation of the solvothermal synthesis of metal-organic frameworks. Multi-dentate organic linkers (orange rods) and metal nodes (red circles) allow for the self-assembly of three-dimensional frameworks under solvothermal conditions

possess four main advantageous properties. First, the coordination of symmetric, repeating units of metal nodes and organic linkers leads to the formation of highly ordered and porous frameworks. Second, MOFs are modular and tunable structures, whose pore size and distribution can be controlled synthetically through variation of the organic linker and to some extent the metal node [27]. Third, some MOF structural motifs, such as the

series developed at the University in Oslo (UiO), represent a robust class of frameworks which display a high degree of stability under a wide range of conditions, especially when using small organic linkers [45]. Finally, MOFs are easily processible with highly crystalline materials being readily prepared from the reaction of metal precursors and organic linkers.

13.3 The Advantages of MOFSCs

The advantages afforded by MOFs can also be applied to DSSCs to overcome the current limitations of molecular dye assemblies. To begin, the porous and highly ordered nature of MOFs allows for the fabrication of thin film devices with exceptional dye loading, reducing both the weight and cost of the device. Expanding on this, if the structure of the MOF can be optimized to allow for fast and efficient exciton transport, the ability to incorporate multiple chromophores into the framework allows for the fabrication of high surface area, thin film, panchromatic electrodes. This, in turn, provides a device which possesses superior dye-loading and spectral overlap when compared to traditional DSSC photoanodes.

In addition, the orientation of the chromophore can be controlled for enhanced energy transfer in processes such as triplet-triplet annihilation-based upconversion (TTA-UC), as well as Förster resonance energy transfer (FRET) and Dexter energy transfer pathways [20, 22, 35, 48]. On a related note, the incorporation of the molecular sensitizer into the organic backbone of the MOF can significantly reduce the detrimental effects of dye aggregation, which is known to shift the absorption of the HOMO-LUMO gap of molecular sensitizers up to 270 meV [13, 41]. Similarly, interactions between neighboring chromophores can lead to static quenching, reducing the quantum yield of the sensitizer emission.

Finally, locking the chromophore into a rigid MOF scaffold allows for exhaustive control over the identity of the chromophore within the sensitizing layer with near molecular precision through a solution processible layer-by-layer (LBL) synthesis also known as liquid phase epitaxy. While LBL growth of MOF films is the most appealing strategy for controlling film thickness and chromophore identity, not all MOFs can be readily fabricated by such methods. Notable examples of some MOFs that can be grown via LBL growth include Hong Kong University of Science and Technology-1 (HKUST-1), surface-integrated metal-organic frameworks (SURMOFs), copper coordinated 5,15-di(p-benzoato)porphyrin, $C_{36}H_{24}N_4O_2[O^-]_2$) $[Cu_x(dbc)_y]$ or zinc coordinated 1,4-benzenedicarboxylate ($C_8H_4O_2[O^-]_2$) $[Zn_x(bdc)_y]$ frameworks, and layered frameworks consisting of porphyrin units supported on molecular "columns" by bridging ligands such as 4,4′-bipyridine ($C_{10}H_8N_2$).

Preliminary examples of such LBL film growth include a mixed-valency ruthenium-based MOF grown via adsorption of ruthenium (III) chloride ($RuCl_3$) precursor and 1,3,5-benzenetricarboxylate ($C_9H_3O_3[O^-]_3$) precursor onto an amine functionalized glass substrate [23]. In addition, LBL deposition has been used to grow the zinc-based framework with (1,4-naphthalene dicarboxylate, $C_{12}H_6O_2[O^-]_2$) and (1,4-diazabicyclo(2.2.2)octane, $C_6H_{12}N_2$) as linkers $[Zn_2(ndc)_2(dabco)_n]$ perfectly

oriented on top of the copper variant, $Cu_2(ndc)_2(dabco)_n$. In this instance, the copper-based framework acts as a template for orienting the zinc-based framework [38]. It is worth noting that in the above example, the placement of the copper framework was necessary to achieve directed growth along the (001) crystallographic plane. When only $Zn_2(ndc)_2(dabco)_n$ was used during the deposition, no unidirectional growth was observed. It will be of interest for future studies to develop new methods which allow for the growth of additional frameworks by LBL methods as it allows for both fine controls over the electrode thickness while maintaining a strong electronic contact with the conductive substrate.

13.4 Potential Considerations of MOFSCs

To date, MOFSCs have displayed maximum power conversion efficiencies (power conversion efficiency, PCEs, or η) of ~ 2.1% PCE in which a cobalt-based framework acts as both a light absorber and hole conducting solid-state electrolyte [1]. More traditional MOFSCs based on liquid junction device architectures typically display efficiencies less than 1%. These stunted efficiencies are directly linked to a few potential challenges, which must be considered when designing MOFSCs. One such challenge involves the diffusion and effusion of the liquid electrolyte within the porous framework. As with current DSSC technology, it is expected that the performance of MOFSCs are dependent on mass transport of the redox electrolyte through the MOF material, with a diffusion of the electrolyte throughout the framework being significantly slower than in bulk solution. The rate of diffusion will be directly dependent on a variety of factors such as the pore size and distribution inherently associated with the MOF material as well as the viscosity, surface tension, and fluid dynamics of the chosen electrolyte.

Yet, despite diffusion being a key challenge for the implementation of MOFSCs, most studies have only looked at the transport of small molecules through MOFs [14, 17, 37, 43]. In these studies, it has been shown that diffusion within the porous framework can be up to four orders of magnitude slower than in bulk solution, commonly taken to be between 5×10^{-5} and 1×10^{-6} cm^2/s [4]. For example, the diffusion of Ce^{4+} within an iridium-modified UiO-67 framework was found to be 1.52×10^{-11} cm^2/s under low concentrations (< 1 mM) and as low as 4.6×10^{-13} cm^2/s at higher concentrations (~ 7 mM) [43]. These values have been attributed in large part to self-exchange between individual Ce^{4+} ions. In addition, these results are in line with molecular dynamics simulations of a lanthanide-copper iodide framework with isonicotinate ($C_6H_4NO[O^-]$) and dimethylformamide (C_3H_7NO) as linkers or coordinative units ($[Ln_3(Cu_4I_4)(ina)_9(DMF)_4]\bullet DMF)_n$, where Ln = praseodymium, Pr; and terbium, Tb), which displayed a calculated diffusion coefficient of I_2 in acetonitrile of 3.8×10^{-9} cm^2/s though no experimental diffusion coefficients were calculated for the MOF [17].

13.5 Fundamental Studies on Charge Separation

Another primary consideration for MOFSC materials involves transport of the photogenerated electron from the site of charge separation through the MOF material to the back contact. While MOFs have displayed the presence of a charge-separated state and photocatalytic activity, they lack an extended band structure typical of other semiconductors like titanium dioxide or zinc oxide [40]. As such, extended electronic communication in MOFs involves a redox hopping mechanism, where a charge is transferred through self-exchange between redox-active linkers. Explanations of the origin of the charge-separated state in some MOF materials have involved simple charge trapping between the metal node and organic linker. In addition, no study has calculated the mobility of free charge carriers during the charge-separated state. Since electronic communication plays an important role in MOFSCs, a discussion of the fundamental studies on both charge separation and redox hopping will follow, below.

We will begin by discussing the former case first. One of the key properties necessary for photovoltaic applications is the ability of the MOF to undergo photoinduced charge separation. Examples of such a charge-separated state can be found in studies probing Metal-organic-framework-5 (MOF-5), Material Institut Lavoisier-125 [MIL-125(Ti), consisting of Ti and terephthalic acid] and its amine-functionalized derivative MIL-125(Ti)-NH_2 [3, 10] (Fig. 13.1). In the case of MOF-5, the presence of a charge-separated state was characterized by visible light irradiation in the presence of methyl viologen ($C_{12}H_{14}[Cl^-][N^+]_2$, V^{2+}) dichloride, a well-known electron acceptor whose radical cation ($V^{\bullet+}$) can be monitored by its distinct absorption spectrum. Upon light irradiation of an aqueous suspension of MOF-5, the characteristic blue color of $V^{\bullet+}$ was detected, demonstrating that MOF-5 is capable of undergoing photoinduced charge-separation.

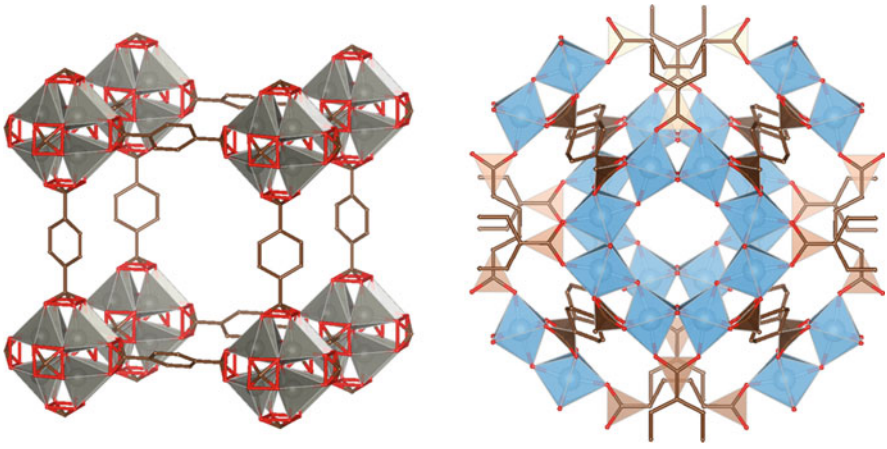

Fig. 13.1 Crystallographic structure of MOF-5 (left) and Mil-125(Ti) (right)

As a follow up to these studies, the highest occupied molecular orbital-lowest unoccupied molecular orbital (HOMO-LUMO) gap of MOF-5 was calculated from diffuse reflectance data and found to be 3.4 eV, only 200 meV larger than the optical bandgap of anatase titania ((TiO_2) (a-TiO_2), the most commonly used semiconductor support in DSSCs. In addition, the LUMO energy could be estimated from photovoltaic cells prepared using MOF-5 supported on fluorine-doped tin oxide (FTO) as a photoanode, in contact with an iodide/triiodide I^-/I_3^- redox electrolyte. During operation of liquid junction DSSCs, the open circuit potential is dictated by the difference in energy between the standard reduction potential of the redox electrolyte, taken to be 300 meV for I^-/I_3^- and the Fermi level energy of electrons in the TiO_2, which can be approximated to the conduction band energy of the semiconductor during normal operation [5]. This same approximation was applied to cells prepared with MOF-5 as the photosensitizer. The open circuit voltage (V_{OC}) of cells prepared using MOF-5 were found to be 300 mV lower than cells prepared with TiO_2. By using TiO_2 reference cells as a standard, with the conduction band energy of TiO_2 taken at -0.1 V versus normal hydrogen electrode (NHE), the conduction band energy of MOF-5 was estimated to be 0.2 V versus NHE. The HOMO energy of MOF-5 was then extracted from the LUMO energy and the diffuse reflectance data and calculated to be 3.6 eV versus NHE. Incidentally, this study suggests the ability of a MOF scaffold to act as a tunable alternative to TiO_2 in photovoltaic devices, where MOFs can accommodate additional sensitizers, which are otherwise limited by their inability to inject excitons into TiO_2.

Regarding MIL-125(Ti) and MIL-125(Ti)-NH_2, the charge-separated states of these frameworks were first characterized by their activity towards alcohol oxidation [9]. Where, adsorption of alcohols (R-OH) into the pores of the framework, followed by ultraviolet (UV) excitation, produced a prominent dark blue color within the sample indicating the formation of titanium (Ti^{3+}). The corresponding alcohol oxidation products were detected via infrared spectroscopy (IR). To identify the active species in this oxidation reaction, electron spin resonance spectroscopy (ESR) was used to probe for the presence of varying metal oxidation states. Interestingly, a Ti^{3+} species was detected after alcohol adsorption and UV excitation, suggesting two possible mechanisms for alcohol oxidation. In the first mechanism, oxidation could occur directly at the Ti^{4+} nodes through reduction of the Ti^{4+} node to Ti^{3+}. In the second mechanism, a photogenerated charge-separated state is generated where Ti^{4+} is reduced to Ti^{3+}, and the hole is centered on the organic linker, which then oxidizes the adsorbed alcohol.

Despite these studies, it wasn't until 2012 that the photophysical properties of this class of frameworks were examined. Garcia et al. began their investigation with transient absorption (TA) techniques and observed that the transient decay of all excited species within the spectrum was coincident, meaning each signal decayed with the same kinetics [10]. The significance of this suggested that the observed spectral features corresponded to either a single species or if multiple species are present, as would be the case if photogenerated electrons were present in the sample, they decayed through interrelated processes such as recombination or annihilation. In addition, the transient species of Mil-125(Ti)-NH_2 decay on the microsecond

timescale, which provides strong evidence for the presence of a charge-separated state [40]. To explore the possibility that such a recombination process was occurring, a simple oxygen quenching study was conducted. In the presence of oxygen, both a decrease in the signal intensity and lifetime of the observed transients was recorded. By taking into consideration the types of species readily quenched by oxygen such as triplet excited states, carbon-centered radicals, and free electrons, it was concluded that the observed transient species was most likely due to photogenerated electrons within the framework. The proposed mechanism for the generation of the charge-separated state is as follows: UV light absorption leads to a charge-separated state with positively charged holes centered on the organic linker, followed by the trapping of photogenerated electrons in the Ti^{4+} node, subsequently reduced to Ti^{3+}. In conjunction with these spectroscopic studies, the presence of a long-lived charge-separated state was again confirmed in the MIL-125(Ti)-NH_2 sample using both methyl viologen ($C_{12}H_{14}[Cl^-][N^+]_2$) and N, N, N′, N′-tetramethyl-p-phenylenediamine (TMPD, $C_{10}H_{16}N_2$) as molecular probes for reduction and oxidation, respectively. As observed in MOF-5, the presence of each corresponding radical cation was detected with both molecular probes.

13.6 Charge Transfer and Redox Hopping

Given the lack of band structure in these materials, it is likely that any photocatalytic activity requiring extended charge transport is promoted by self-exchange or "redox hopping" between redox active moieties incorporated into the MOF scaffold. A schematic representation is illustrated in Fig. 13.2.

Examples of charge transport via a redox hopping mechanism have been observed before in polymer materials [19, 34] and examples of such charge transfer mechanisms within MOFs are readily available in the literature [2, 7, 15, 16, 26]. The first reported example of redox hopping in MOFs was by Morris et al. who demonstrated the electrical conduction of a cobalt framework with [5,10,15,20-tetra(4-carboxyphenyl)porphyrin, Co^{III}TCPP, $C_{45}H_{30}N_4O_8$] secondary building units, and Co^{III}TCPP struts bound by linear trinuclear Co^{II}-carboxylate film [Co(RCOO)n, CoPIZA] in the form of ($Co^{3+/2+}$TCPP/CoPIZA), deposited on fluorine-doped tin oxide substrate (FTO). The CoPIZA/FTO could not be explained by a simple band theory argument. Instead, the observed electrical conductivity was attributed to redox hopping between CoTCPP units, which act as support struts for the CoPIZA framework [2]. For such a mechanism to exist, it relies on two assumptions. First, the active redox centers which participate in charge transport must have the same or similar redox potentials for electron transfer to occur. Second, the redox active sites must lie in close enough proximity to allow for efficient redox hopping. If both conditions are met, then the electrical conductivity of the material can be described by charge hopping from one redox center to another, giving rise to Fickian diffusion of electrons through the material.

Characterization of such materials is commonly conducted using electrochemical methods. For any redox active species, such as those immobilized in the CoPIZA

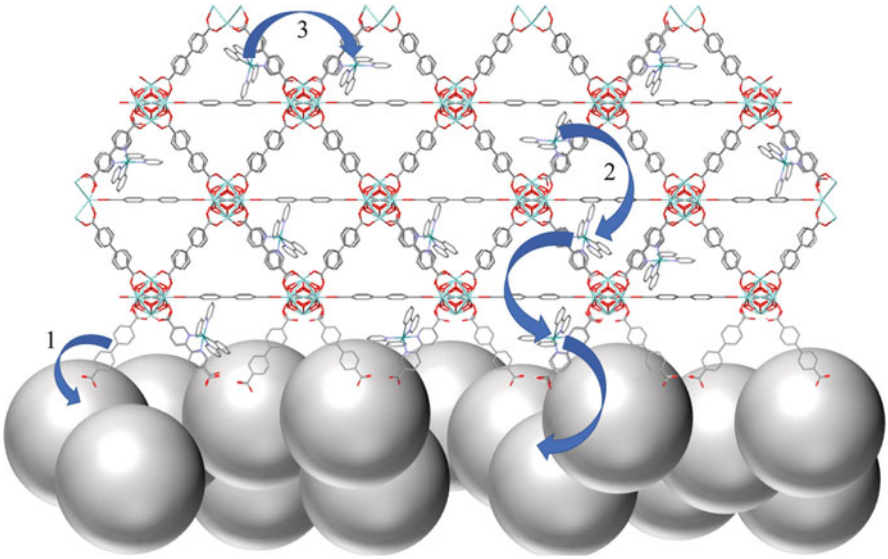

Fig. 13.2 The generation of charge-separated states via the redox hopping mechanism. In this case, a ruthenium coordination complex Ruthenium(II) bis-2,2′-bipyridine [$C_{10}H_8N_2$] 5,5′-dicarboxy-2,2′-bipyridine [$C_{12}H_8N_2O$] ($Ru(bpy)_2(dcbpy)^{2+}$) has been incorporated into the backbone of the MOF scaffold. Charge separation occurs through two processes: the direct excitation of the 5,5-′-dicarboxy-2,2′-bipyridine linker which then injects directly into the titania (TiO_2) semiconductor (process 1), or through excitation and injection of a ruthenium species incorporated into the backbone of the MOF scaffold (process 2). Exciton diffusion throughout the framework typically occurs through redox hopping between the incorporated ruthenium centers before injection or recombination with a positively charged hole (process 3)

framework, the electrochemical response is dependent upon the diffusion coefficient of the redox active species (D), and thus for an immobilized species, the rate of charge transfer (k_{ct}, unit s^{-1}). For such materials, there exist three regimes: (i) the rate of charge transfer (k_{ct}) is faster than the experiment sweep rate (ν, unit mV/s) or $k_{ct} > \nu$, (ii) $k_{ct} \approx \nu$, and (iii) $k_{ct} < \nu$. The first regime describes rapid charge transport, where for immobilized species, the cyclic voltammogram will display asymmetrical shape ($\Delta E_p = 0$ mV) centered at the reduction potential of the material. Chidsey's work on surface-modified gold electrodes represents a classic example of such work [8]. Since the electrochemical response of the CoPIZA framework exhibits non-zero scan rate dependence across all measured scan rates, it was concluded that for the CoPIZA/FTO film, regime (iii) most accurately describes its electron transfer kinetics. Since the electron transport is sluggish in this regime, the behavior of the cyclic voltammogram exhibits the same behavior for freely diffusing redox active species in solution, and this follows the Randles-Sevcik equation (Eq. 13.1).

$$i_p = 0.4463nFAC\left(\frac{nF\nu D}{RT}\right)^{\frac{1}{2}} \tag{13.1}$$

In the above equation, i_p is the peak current of either the background corrected anodic or cathodic process (A), n is the number of electrons transferred in the redox active process (dimensionless, usually one), F is Faraday's constant (96485.3 C mol^{-1}), A and C are the active area of the electrode (cm^2) and the bulk concentration of the redox active species (mol/cm^3), v is the scan rate (mV/s), R and T are the ideal gas law constant (K^{-1} mol^{-1}), and the temperature (K), and D is the diffusion coefficient of the species (cm^2/s). By varying the scan rate of the cyclic voltammogram, and generating a plot of peak current versus the square root of the scan rate, a linear relationship can be observed whose slope is equal to 2.69×10^5 $ACD^{1/2}$ for a one-electron redox couple measured at 25 °C. From this data, the diffusion coefficient can be calculated for the redox active species.

For immobilized species incorporated into the MOF, however, a more reliable method for determining the diffusion coefficient can be employed through the analysis of spectroelectrochemistry. From the spectroelectrochemical data, it was shown that the reduction processes observed within the film were ascribed to both the $Co^{3+/2+}$ redox couple and the $Co^{2+/+}$ redox couple. From these results, the apparent diffusion coefficient for redox hopping throughout the CoPIZA film (D_{app}, unit cm^2/s) was measured using time-resolved spectroelectrochemistry data and a modified version of the Cottrell equation (Eq. 13.2). For the CoPIZA material, D_{app} was calculated to be 7.55 ($\pm$0.05) $\times$ 10^{-14} cm^2/s. Ultimately, this value is found to be four to six orders of magnitude lower than for modified polymer films which are typically on the order of ~10^{-8}–10^{-6} cm^2/s [32, 39, 44]. This significant reduction in D_{app} could be attributed to reduced diffusion of ionic species within the framework leading to significant impacts on the rate of charge transport within the MOF film [26].

$$\Delta A = \frac{2A_{\max}D_{app}^{1/2}t^{1/2}}{d\pi^{1/2}} \tag{13.2}$$

Likewise, Hupp et al. showed that charge transport via redox active linkers can be separated from chromophores by incorporation of additional redox active moieties inside the framework itself [15]. By incorporating the ferrocene derivative, ferrocene carboxylic acid, into the open channels of the framework Northwestern University-1000 [NU-1000], the authors demonstrated bias-switchable redox behavior in which oxidation of the tethered ferrocene units selectively blocked cation mobility within the NU-1000 pores. By blocking the pores in such a manner, the authors were able to remove any observable redox chemistry for the pyrene-containing linkers. Upon reduction of these ferrocene units, the cation mobility of the supporting electrolyte was restored, as well as the electrochemical response of the pyrene-containing linker. In a follow-up study, the authors demonstrated that by utilizing host-guest chemistry, the electron transfer kinetics and the apparent diffusion coefficient for redox hopping could be modulated. By taking advantage of the high affinity for β-cyclodextrin (β-CD, $C_{42}H_{70}O_{35}$) complexation with ferrocene and the low affinity for

complexation of β-CD with ferrocenium ($C_{10}H_{10}$[X-][Fe^{+}], where X^{-} is the counter anion), the authors were able to observe [$Fe(C_5H_5)_2$], modulated redox hopping as a function of β-CD concentration, with a 30-fold reduction of D_{app} at the maximum solubility of the β-CD. The apparent diffusion coefficient can also be directly related to the microscopic rate constant for redox hopping events k_{hop} (Eq. 13.3).

$$k_{hop} = \frac{D_{app}}{r^2} \tag{13.3}$$

In the case of the functionalized NU-1000 framework, inductively coupled plasma mass spectrometry (ICP-MS) and coulometric analysis supports the assumption that one ferrocene molecule is present at each node of the framework. This provides a ferrocene-to-ferrocene separation distance of 1.6 nm, which in turn resulted in a reduction of k_{hop} from 780 s^{-1} in the absence of β-CD, to 23 s^{-1} when the β-CD concentration is 20 mM. However, in either of these cases, the rate of k_{hop} is still dependent on the diffusion of either cations or anions of the electrolyte throughout the framework.

13.7 Literature Examples of MOFSCs

One of the most common frameworks employed in MOFSCs is the pillared porphyrin framework. The most notable entry in this class of MOFs is the pillared porphyrin framework 4 (PPF-4), which consists of layered structure of tetra(carboxyphenyl) porphyrin (TCPP, $C_{48}H_{28}N_4O_8Zn$) linker molecules with planar coordination to zinc (Zn^{2+}) ions and separated by 4,4′-bipyridine ($C_{10}H_8N_2$) linkers (Fig. 13.3). In this configuration, the framework acts as a series of two-dimensional layers of planar Zn-TCPP units joined by vertical bipyridine pillars. One of the most notable studies involving this framework examined the photovoltaic properties of cells prepared with PPF-4 as its sensitizer. The importance of these studies was that the observed photovoltaic response was due solely to the PPF-4 framework acting as the photosensitizer on a TiO_2 scaffold [41]. By using only prewashed nanocrystals of PPF-4 dispersed on a conductive substrate coated with TiO_2, the authors were able to prepare cells where it was not possible for free linker molecules to coordinate to TiO_2 and contribute to the cell's photocurrent response. This approach differed from traditional methods of film preparation wherein the MOF film is grown in situ solvothermally on the titania/fluorine-doped tin oxide (TiO_2/FTO) electrode surface, which leads to ambiguity as to whether the framework is acting as the sensitizer in the MOFSC, or if the photovoltaic properties are due to chemisorbed linker molecules on the TiO_2 working electrode.

To begin, nanocrystals of PPF-4 were synthesized in a one-pot reaction from Zn-TCPP, zinc nitrate tetrahydrate [$Zn(NO_3)_2$•$4H_2O$], and 4,4′-bipyridine ($C_{10}H_8N_2$) in 1:3 (v:v) ethanol (C_2H_6O) and diethylformamide (DEF, HCON$(C_2H_5)_2$) solution. The resulting crystals were subsequently collected and washed via centrifugation with DEF and ethanol. These crystals were then dispersed in

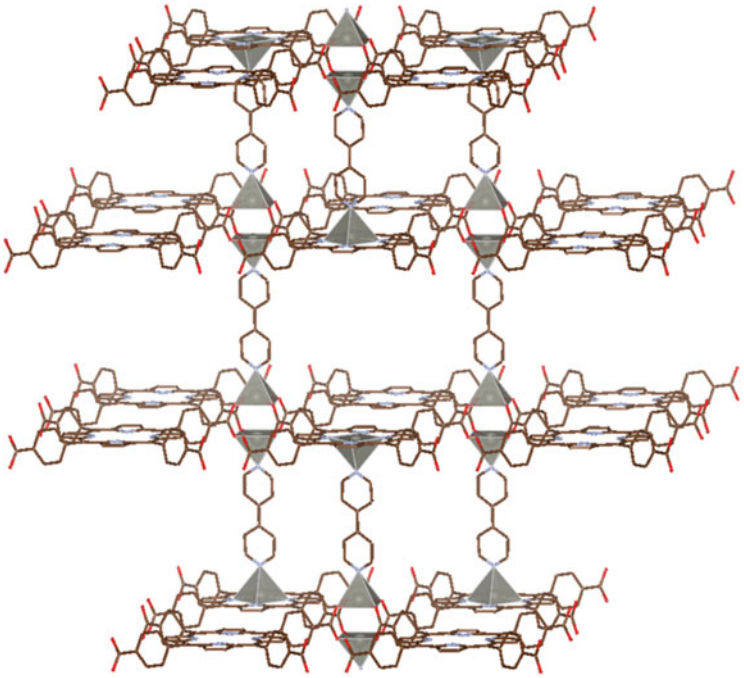

Fig. 13.3 Crystallographic structure of PPF-4 displaying the characteristic layered TCPP units joined by 4,4′-bipyridine pillars

chloroform and drop-cast onto a TiO_2-coated substrate to form the PPF-4/TiO_2 working electrode. This working electrode was sealed together with a platinum (Pt)-FTO counter electrode and iodide-based electrolyte. The photovoltaic properties the prepared cells are shown below (Fig. 13.4).

From the current-voltage plots in Fig. 13.4, a clear increase in photocurrent response is observed by PPF-4 over TiO_2. When a 450-nm band-pass filter was used to remove the photoresponse from UV-excited TiO_2, a prominent contribution from the PPF-4 is observed, while the TiO_2 control electrode exhibits a photovoltaic response nearly identical to the prepared PPF-4 cell under dark conditions. Ultimately, due to the absence of a strong electronic contact in this device architecture, the overall cell efficiencies were only 2.3×10^{-3}%. In addition to the current-voltage plots, electrical impedance spectra (EIS) demonstrate a reduction in the electron transfer resistance across both PPF-4 MOFSCs and TiO_2 control. However, the cells prepared with PPF-4 as the sensitizer displayed consistently lower electron transfer resistance than those of the TiO_2 control. These results demonstrated unambiguously that the PPF-4 MOF nanocrystals act as the sensitizer for the MOFSC with no additional contributions from adsorbed linker or TiO_2 photoexcitation. More importantly, this study provided the first proof-of-concept MOF/TiO_2 electrodes for light-absorbing chromophores in photovoltaic applications.

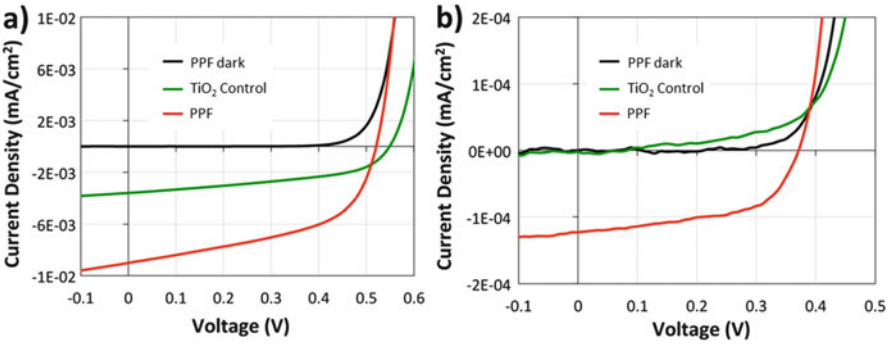

Fig. 13.4 A photovoltaic response of PPF-4 MOFSCs prepared via drop-casting of PPF-4 on TiO_2 under AM 1.5 simulated illumination (**a**). The photovoltaic response of PPF-4 MOFSCs under 450 nm band-pass filtered illumination to remove UV-excited photoresponse from TiO_2 (**b**). (Reprinted (adapted) with permission from Spoerke et al. [41]. Copyright 2017 American Chemical Society)

Similar porphyrin-based frameworks aim to alleviate another significant challenge faced by MOFSCs: the reduction of deleterious recombination processes between the redox electrolyte and the photogenerated electrons within the MOF framework [12]. It was, therefore, reasoned that if the photogenerated holes could be quickly and efficiently transported to the periphery of the MOF film where the electrode/electrolyte interface exists, then exclusion of the redox electrolyte from the pores of the MOF would lead to a reduced chance for unwanted electronic recombination. In addition, one of the major considerations for the design of novel frameworks for MOFSCs is the enhancement of the photogenerated electron diffusion distance (L_d). In general, this kind of enhancement can be achieved through two strategies – through the optimization of three-dimensional frameworks to allow for rapid exciton transport through the extended MOF structure, or through collapsing a three-dimensional, layered framework, into a two-dimensional framework. Regardless of which strategy is chosen, the overall goal is the same, to bring the chromophore linkers of the MOF in close Van der Waals contact with one another, allowing for the exchange of excitonic energy more readily.

As one example of the latter strategy, work by Hupp et al. with a derivative of the PPF-4 framework employing metallated zinc(II) meso-tetra(4-carboxyphenyl) porphyrin (Zn-TCPP) was selectively collapsed from its three-dimensional structure into a layered two-dimensional structure using solvent-assisted linker exchange (SALE) [12]. In SALE, the MOF is soaked in a solution containing a separate linker or coordinating unit which can then undergo ligand exchange with some of the organic linkers in the MOF backbone. In this case, a collapse of the framework brings the Zn-TCPP units in closer Van der Waals contact than in the pillared configuration increasing k_{hop} for *inter*-layer electron transfer. That is to say, the rate of electron transfer between two independent layers increases. The increase in the *inter*-layer k_{hop} leads to an increase in L_d, as *inter*-layer electron transfer will bring either a photogenerated electron closer to the TiO_2 scaffold, or a

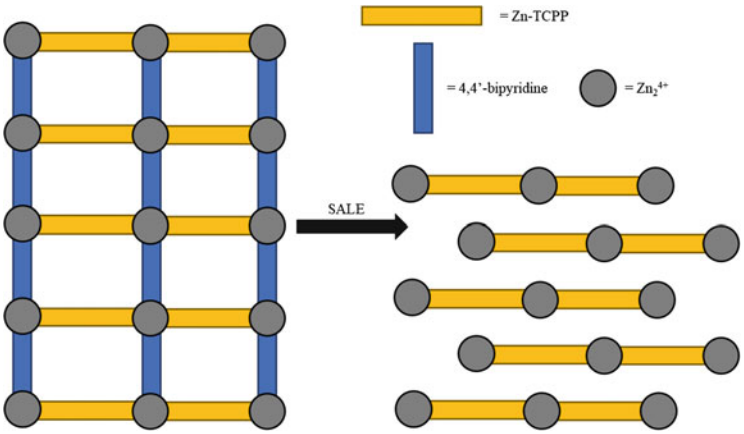

Scheme 13.3 The collapse of a layer-by-layer Zn-TCPP PPF by SALE to produce a layered two-dimensional MOF

photogenerated hole closer to the electrode/electrolyte interface. In contrast, *intra*-layer hopping, hopping within a single layer between Zn-TCPP units, produces largely no beneficial effect for increasing L_d.

In this instance, the pillared Zn-TCPP framework was soaked in a solution of pyridine to remove the bipyridine pillars. When this process is carried out, the pillared morphology of the framework was collapsed, such that the orientation of the film would resemble that of a layered two-dimensional coordination polymer (Scheme 13.3).

Pyridine was chosen as it possesses a slightly higher pK_a than that of 4,4′-bipyridine (5.25 vs. 4.9), allowing for the near-quantitative exchange of the 4,4′-bipyridine pillars. The *post*-SALE films were characterized by both profilometry and ellipsometry to determine the new film thickness and density. Measurements of the film thickness supported an average decrease from approximately 80 nm to approximately 40 nm after SALE. In addition, collapsing such films led to direct increases in film density and, therefore, the refractive index (n) of the material. Since the refractive index of a porous framework can be estimated as a volume-weighted average of the indices for the framework itself ($n_{MOF} > 1$, dimensionless) and the corresponding void space within the MOF ($n_{vac} = 1$), the observed increase in the refractive index from the native structure to the collapsed film (1.4–1.8) indicated an approximate doubling of the film density. For these methods to be expanded upon, it will be crucial in follow-up studies to conduct in-depth materials characterization of the framework *pre*- and *post*-SALE.

To examine the enhanced excitonic transport properties of the collapsed film, a molecular quencher was installed atop the framework prior to collapse. For this purpose, a standout candidate that could easily be incorporated by an LBL approach was the palladium-metallated porphyrin (Pd-TCPP) which is known to quench the excited state of the Zn-TCPP linker [6]. By installing two layers of Pd-TCPP on top

of films prepared with 13 cycles of Zn-TCPP and 4,4′-bipyridine layers, the emission intensity of the Zn-TCPP linkers was quenched by approximately 50%. Post-collapse however, this quenching efficiency increased to approximately 70%, qualitatively indicating an increase in exciton transport distance via *inter*-layer hopping to the Pd-TCPP quenchers. From this assessment, an estimate of L_d was derived by equating the percentage of quenched emission to the percentage of Zn-TCPP linkers capable of being quenched by Pd-TCPP, whether by direct energy transfer or by *inter*-layer hopping between Zn-TCPP units. For this approximation, two assumptions must hold true. The first being that the rate of quenching of the Zn-TCPP units by Pd-TCPP is fast relative to the nonradiative decay of the excited Zn-TCPP units, and the second being the optical density of the film is small enough that the probability of photon absorption by any individual Zn-TCPP unit is independent of its location within the film. Based on these assumptions, prior to film collapse, an exciton could readily diffuse across a maximum of eight layers. Post-collapse however, this number increased to a maximum of 11 layers.

As a follow-up study, Hupp and coworkers have also investigated replacing the 4,4′-bipyridine units of this framework, with smaller bifunctional organic linkers which will maintain the three-dimensional nature of the framework while reducing the distance between individual Zn-TCPP units [11]. In this work, 1,4-diazobicylco [2.2.2]octance (DABCO) was exchanged with the 4,4′-bipyridine struts through SALE. In doing so, the authors demonstrated that the number of layers the exciton could traverse was increased from 11 layers to 26. This substantial increase was due to the three-dimensional structure of the framework, which forces the Zn-TCPP units to sit facially aligned with each other, while in the collapsed two-dimensional topology, the Zn-TCPP units adopt a staggered arrangement leading to almost no decrease in the electronic coupling distance between porphyrin units. As such, only a marginal increase was observed when pyridine (C_5H_5N) was used to replace 4,4′-bipyridine. Ultimately, these studies clearly demonstrate that post-synthetic modification of current frameworks could be utilized to improve device performance.

In moving away from porphyrin-based MOFs, other investigators have characterized MOFSCs utilizing MOF sensitizers in which the aromatic linker, typically 1,4-benzene dicarboxylic acid (bdc, $C_8H_6O_4$) acted as the light absorber. Probably the most well-studied case for such a system is the commercially available framework aluminum coordinated benzene dicarboxylic acid [$Al_2(bdc)_3$]. The structure of $Al_2(bdc)_3$ can be simply described as a zinc oxide [Zn_4O] cluster bridged by benzene dicarboxylic acid linkers (Fig. 13.5a). However, as discussed earlier, the HOMO-LUMO gap for such a framework is ill-matched to the visible spectrum ca. 3.4 eV [3]. Cells utilizing $Al_2(bdc)_3$ as their sensitizer were fabricated by spin coating $Al_2(bdc)_3$ framework onto a TiO_2 photoanode supported on indium-doped tin oxide (ITO). A hole conducting layer of Spiro-OMeTAD ($C_{81}H_{68}N_4O_8$) was spin-coated on top of the photoactive MOF layer, followed by deposition of a gold counter electrode. Though revolutionary at their introduction, the current-voltage performance of these devices displayed poor percent power conversion efficiencies (% PCE) with a maximum % PCE of ~0.002% for 2.7 μm films (Fig. 13.5b).

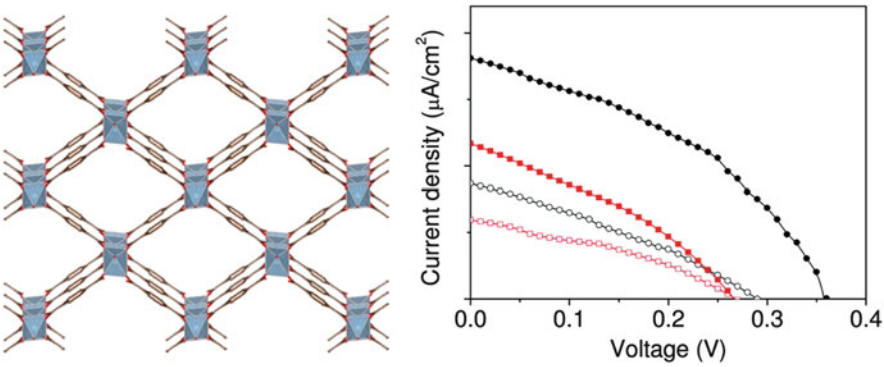

Fig. 13.5 Crystallographic structure of $Al_2(bdc)_3$ as viewed down the b axis displaying one-dimensional rhombohedral channels (**a**). Photocurrent response of cells prepared with $Al_2(dbc)_3$ as the sensitizer and Spiro-OMeTAD as the hole conductor with a gold counter electrode with either $Al_2(bdc)_3$ sensitizer with a thickness of 2.7 μm (red solid squares) or 5.4 μm (red open squares) or with DMB@$Al_2(dbc)_3$ sensitizer with a thickness of 2.7 μm (black solid circles) or 5.4 μm (black open circles) under AM 1.5 illumination (**b**). (Reprinted (adapted) with permission from Lopez et al. [49]. Copyright 2011 American Chemical Society)

To mitigate these low efficiencies, $Al_2(bdc)_3$ was doped with 1,4-dimethoxybenzene (DMB, $C_8H_{10}O_2$) which acts as a hole-trapping agent to produce the framework DMB@$Al_2(bdc)_3$. By incorporating a hole-trapping agent into the framework, the lifetime of the charge-separated state could be enhanced reducing parasitic recombination within the cell. Indeed, by incorporating DMB into the framework, the lifetime of the transient corresponding to free electrons (optical absorption from 350 to 500 nm) increased markedly. In addition, by incorporating these deep trap states into the framework, an increase in fill factor (*ff*) was observed for cells prepared with DMB, which increased by 6.62% from 33.84% to 40.46% (Fig. 13.5b). This, in turn, led to a substantial boost in the relative device % PCE up to ~ 0.005% PCE under optimal conditions. More importantly, this study laid the groundwork for the design of state-of-the-art MOFSCs, leading investigators to consider the modification of the MOF linker as a suitable site for the incorporation of a photosensitizing chromophore to compensate for poor spectral overlap of the framework itself with solar irradiance.

More successful solar cells, however, were prepared with an iodine-doped Cu-MOF, formed by the reaction of $Cu(NO_3)_2$ with benzene-1,3,5-tricarboxylate, acting as a replacement for more traditional DSSC chromophores (Fig. 13.6) [24]. By utilizing Cu-MOF as their sensitizer, cells prepared by LBL growth of Cu-MOF on TiO_2-coated fluorine-doped tin oxide (TiO_2/FTO) substrates displayed % PCEs of 0.008% PCE. To further enhance cell performance, iodine was doped into the framework. The benefit of this additive is twofold. First, incorporation of iodine molecules into the framework switches the electrical conductivity of the framework from the insulating regime to the semiconductive regime through either partial oxidation of the Cu-MOF or conduction through an ordered iodine network in the framework [21, 46]. Impedance spectroscopy

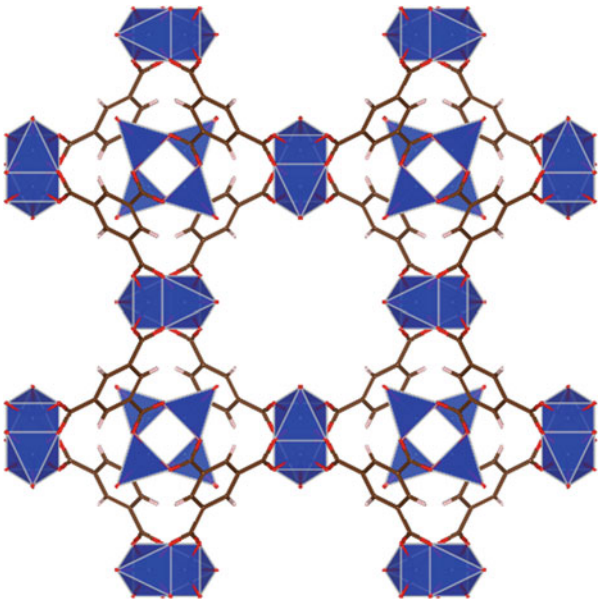

Fig. 13.6 Structure of Cu-MOF as viewed down the crystallographic *a* axis

was used to determine the effect of iodine doping on the conductivity of the framework. From the EIS spectra, it is clear that doping the framework with iodine significantly improves the conductivity of the framework under solar irradiance (Fig. 13.7a). It was observed that the charge transfer resistance (R_{ct}) of the iodine-doped Cu-MOF is one order of magnitude lower than TiO_2/FTO (Fig. 13.7b), and three orders of magnitude lower than Cu-MOF/TiO_2/FTO (Fig. 13.7c). Finally, R_{ct} was investigated for iodine-doped Cu-MOF under dark and illuminated conditions (Fig. 13.7d). The drastic decrease in R_{ct} under illumination suggests that upon illumination, iodine-doped Cu-MOF acts as a photosensitizer generating electron-hole pairs on illumination which are rapidly injected into the TiO_2 support.

In addition to the impressive change in conductivity, iodine doping also increased the efficiency of the device by an order of magnitude increasing the % PCE from less than 0.01% PCE to 0.26% PCE. However, there is one major caveat to improving the device performance with iodine, and that is that iodine is well-known to undergo photoinduced dissociation into the radical species ($I^{\bullet}$) under visible illumination (Eq. 13.4). In these circumstances, it is unclear whether the Cu-MOF acts independently as a sensitizer for the PV, or if the photogenerated $I^{\bullet}$ radical contributes appreciably to the device performance by reacting with the TiO_2 semiconductor.

$$I_2 \xrightarrow{h\nu} 2I^{\cdot} \tag{13.4}$$

In terms of modifying the MOF linker itself to incorporate various chromophores, few examples exist in the literature. One instance can be found in the work presented

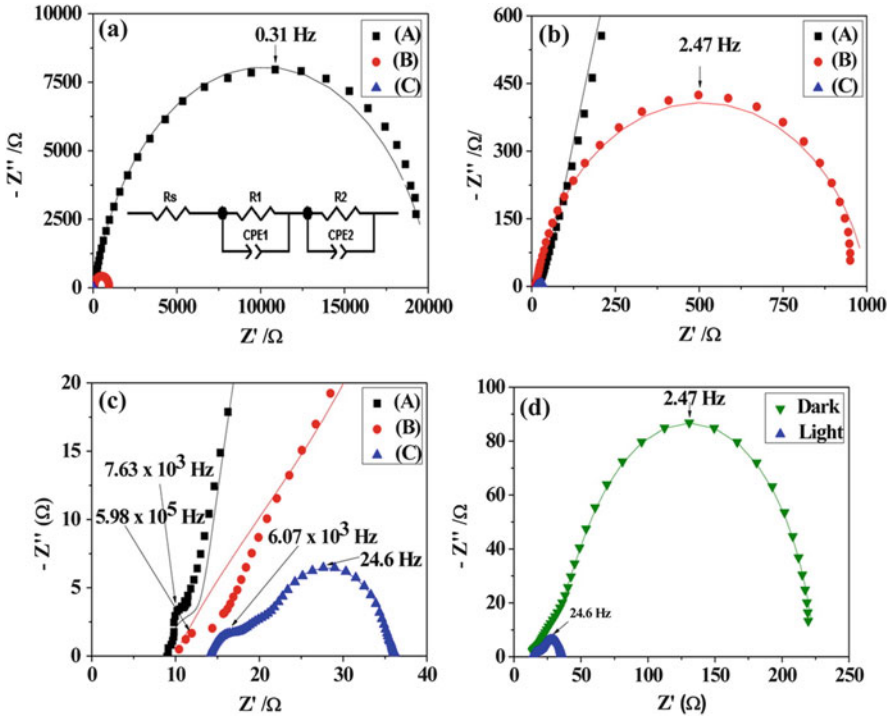

Fig. 13.7 (**a**) Circuit model and impedance spectrum of cells prepared with either (A) undoped Cu-MOF/TiO_2/FTO (black squares), (B) TiO_2/FTO (red circles), or (C) iodine-doped Cu-MOF/TiO_2/FTO (blue triangles) under simulated AM 1.5 illumination. (**b**) Zoomed in impedance spectrum of (A) at higher frequencies emphasizing the insulating nature of the undoped Cu-MOF framework relative to that of TiO_2/FTO. (**c**) Zoomed-in impedance spectrum of (A) at the highest frequency region. (**d**) Electrical impedance spectrum of iodine-doped Cu-MOF/TiO_2/FTO cells under dark and simulated AM 1.5 illumination. (Reprinted (adapted) with permission from Lee et al. [24]. Copyright 2014 American Chemical Society)

by Morris et al. utilizing a ruthenium [Ru(II)L_2L'] (L = 2,2′-bipyridine, $C_{10}H_8N_2$; L′ = 2,2′-bipyridine-5,5′-dicarboxylic acid, $C_{12}H_8N_2O_4$) (RuDCBPY) linker to form a RuDCBPY-doped UiO-67 framework (UiO-67(Ru)) [29]. Cells sensitized with UiO-67(Ru) were prepared using two methods, wherein UiO-67(Ru) was grown either directly via solvothermal synthesis onto TiO_2/FTO, termed UiO-67(Ru)-OP/TiO_2/FTO (OP = one pot), or by post-synthetic modification of pristine UiO-67 grown directly onto TiO_2/FTO by submerging the prepared films in an ethanolic solution of RuDCBPY termed UiO-67(Ru)-PS/TiO_2/FTO (PS = post-synthetic).

When grown directly onto FTO, at low-doping concentrations of RuDCBPY, it was found that the UiO-67(Ru) framework displayed excited-state properties consistent with the RuDCBPY linker dissolved in DMF. These excited-state characteristics include a long-lived metal-to-ligand charge transfer state (MLCT) with a lifetime of ~ 1.4 μs [29]. By increasing the doping concentration, a decrease in the

emission lifetime was observed, corresponding to homogenous energy transfer between RuDCBPY centers [30]. Additionally, this framework readily grows on TiO_2 scaffolds without appreciably changing the energetics of the RuDCBPY linkers relative to RuDCBPY in solution [28]. Based on these observations, this framework represented a strong candidate for use in photovoltaic applications.

Cells prepared using the UiO-67(Ru) framework as a sensitizing material displayed moderate photocurrents with short-circuit current densities (J_{sc}) ranging from 0.03 to 0.54 mA/cm^2 and open-circuit potentials (V_{OC}) ranging from 370 to 520 mV when utilizing a common I^-/I_3^- electrolyte. In addition, cells displayed higher amounts of charge recombination than traditional DSSCs with the average fill factors (*ff*) across the cells being 0.50. These *ff* values were presumably due to partial occlusion of the pores to I^- and I_3^- diffusion as well as large film thickness which can prevent the majority of excitons from reaching the TiO_2 scaffold. Evidence for such an event can be seen in cells prepared using the post-synthetically modified UiO-67(Ru) films. In a post-synthetic modification, only the outermost layers of the UiO-67 framework are likely to undergo efficient linker exchange. This was confirmed by confocal fluorescence microscopy which showed denser populations of RuDCBPY centers along the edges of the UiO-67 crystallites. When such a buildup occurs, the high density of RuDCBPY units along the exterior of the MOF film leads to exclusion of the redox electrolyte from the interior of the MOF, resulting in lower *ff* values.

Another downfall of these devices was the lack of control over film thickness, which resulted in a reduction in the efficiency of charge collection. For example, the maximum hopping distance for photogenerated electrons in this material can be calculated form k_{hop} (unit Angstrom) by the following equation (Eq. 13.5).

$$k_{hop} = \frac{mD_{RET}}{R_{hop}^2} \tag{13.5}$$

In this equation, m is a dimensional factor (unitless, where $m = 6$ for three-dimensional systems, $m = 4$ for two-dimensional systems, and $m = 2$ for one-dimensional systems), D_{RET} is the diffusion coefficient for energy migration (cm^2/s) in crystalline $Ru(bpy)_3^{2+}$ salts [18]. From this data, it was calculated that the maximum hopping distance for RuDCBPY-UiO-67-TiO_2 of 254 Å. This distance was significantly smaller than the average film thickness of ~10 μm as calculated from scanning electron microscopy (SEM) images. As a consequence, the maximum % PCE observed for the prepared cells was only measured to be 0.125%. Notably, however, UiO-67(Ru) outperformed control cells constructed in this study in which RuDCBPY adsorbed directly onto TiO_2 or those in which UiO-67 acted as the sensitizer. This study highlights some of the challenges and future considerations that will be discussed at the end of this chapter. Namely, the need for control of MOF film growth and transport of redox mediators through control of the MOF three-dimensional (3D) structure.

In efforts to minimize the diffusion limitation inherent in many MOF materials, some investigators have shifted their focus toward solid-state MOFSCs. These cells

eschew traditional liquid electrolytes in favor of hole conducting polymers or MOF materials. Possibly one of the most notable efforts to fabricate a MOFSC utilizes a hole-conducting MOF based on the coordination between cobalt (Co^{2+}) ions and a redox active linker, di(3-aminopropyl)-viologen (DAPV, IUPAC Name 1 1,1′-bis (3-aminopropyl)-[4,4′-bipyridinium] dianion, $C_{16}H_{24}[X^{-}]_2N_2[N^{+}]_2$), to form the framework Co-DAPV [1]. Hall-type measurements of the Co-DAPV MOF displayed a [positive] *p*-type photoconductance with a hole concentration and hole mobility of 3.35×10^8 cm^3 and 0.017 $cm^2/V•s$ respectively. These mobilities are on par with poly(3-hexylthiophene-2,5-diyl) (P3HT, $(C_{10}H_{14}S)_n$) doped with 2,3,5,6-Tetrafluoro-7,7,8,8-tetracyanoquinodimethane (F_4TCQN, $C_{12}F_4N_4$), an oxidant used to increase the conductivity of organic semiconductors [36]. The origin of such photoconductivity is attributed to metal-to-ligand charge transfer involving the transfer of photoexcited electrons from the cobalt metal center to the DAPV ligand.

Films of Co-DAPV were grown on TiO_2 using LBL techniques, and in doing so, a [positive-negative] p-n heterojunction is prepared, which led to a maximum power conversion efficiency of 2.1% PCE (Fig. 13.8). In terms of device performance, the prepared cells displayed J_{sc} values, ranging from 0.98 to 4.92 mA/cm^2 for cells prepared with 5 and 15 LBL cycles of Co-DAPV, respectively. Likewise, The V_{OC} values achieved a maximum of 670 mV when 15 layers of Co-DAPV were deposited on the electrode surface. It is worth noting that up to 30 LBL cycles were performed on some devices, but when 15 layers were exceeded, a reduction in J_{sc} was observed, while the V_{OC} values remained unchanged. The increase in J_{sc}, up to 15 cycles and subsequent reduction in J_{sc} above 15 cycles was correlated to a reduction in the charge transport resistance (R_{trans}) within the Co-DAPV film. Ultimately, by combining the light absorbing layer and the hole conducting layer into a single material, the classical challenges of electrolyte diffusion and hole mobility have been

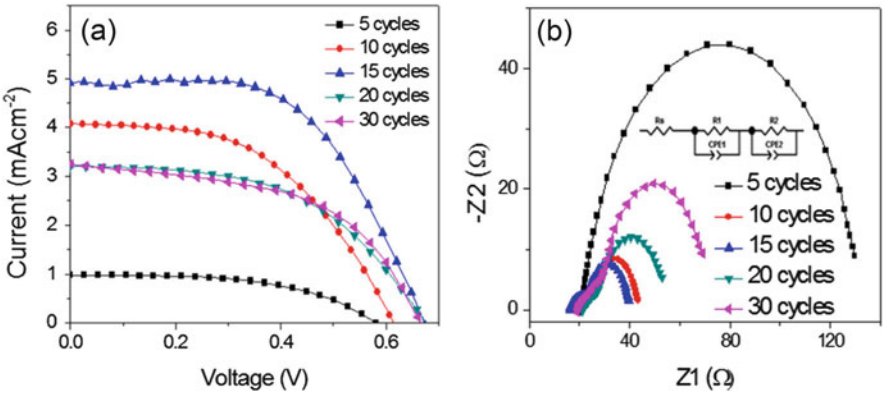

Fig. 13.8 (Left) Photocurrent response of MOFSCs prepared using Co-DAPV as both the sensitizer and hole conductor as a function of layer-by-layer cycles. (Right) Nyquist plot of prepared cells under 0.1 sun illumination displaying the increase in conductivity of the Co-DAPV MOF up to 15 LBL cycles. (Reprinted (adapted) with permission from Ahn et al. [1]. Copyright 2017 American Chemical Society)

alleviated allowing for the preparation of high-efficiency devices. Moving forward, considerable interest should be given to developing and optimizing solid-state MOFSCs as the absence of comparative cells for this architecture is currently lacking within the literature. Additionally, designing novel hole-conducting MOFs capable of fast and efficient redox hopping to improve hole mobility with absorption profiles well-suited for visible and near-infrared light absorption should receive consideration as well.

13.8 Conclusions and Future Outlook

Given the preliminary work discussed herein, it is suitable to provide a perspective of the field and future considerations for MOFSCs and their implementation. To begin, three major challenges must be addressed for the field to advance. First, the development of new MOF materials, which possess efficient exciton transport is essential to improve photogenerated electron and hole transport through the MOF. Significant progress has been made by utilizing dopants such as iodine or redox active ligands like DAPV to improve exciton transport throughout the MOF sensitizer. However, additional studies are needed to fully realize a highly photoconductive material, which possesses satisfactory exciton diffusion. This can be accomplished through the development of modified organic linkers, which possess rapid self-exchange rate constants and long-lived charge-separated states. Likewise, host-guest interactions can also be exploited to promote increased exciton diffusion by incorporating additional trap states, which can reduce exciton recombination and should evolve coincidently with the design philosophy of increased photo-conductivity.

Second, new studies to enhance the diffusion of the redox electrolyte throughout the MOF are necessary. For rapid and efficient chromophore regeneration, the redox electrolyte must be able to freely diffuse into and out of the framework. As such, framework engineering and design should account for and aim to improve electrolyte diffusion. This can be accomplished through modification of existing frameworks with large channels such as the HKUST-1 and NU-1000 frameworks, or by the development of novel frameworks unlike those presently studied. Considerations such as pore obstruction by incorporated chromophores, channel, pore orientation, and defect density will be primary research goals.

Finally, the growth and modification of MOF films must lead to strong electronic contacts to the TiO_2 scaffold. This is a necessity for rapid injection of electrons into TiO_2 as well as leading to uniform coverage of the TiO_2 scaffold. Most MOFSCs can be prepared by loading the MOF sensitizer onto the TiO_2 either by solvothermal growth, spin coating, or by LBL deposition. While LBL growth is preferred, not all MOFs can be easily fabricated on the surface of TiO_2 through LBL methods. While most other MOFs can be prepared via solvothermal synthesis, this method of film growth affords virtually no control over film thickness. This lack of control only helps to exacerbate the diffusion limitations of prepared devices, despite the presence of strong electronic contacts between MOF film and the conductive substrate.

Contrarily, spin-coating the MOF sensitizer allows for excellent control of film thickness but leads to poor electronic contact between the MOF and TiO_2 as growth is not directly seeded from the surface as it is in both LBL growth and solvothermal synthesis. This leads to poor injection rates for the photogenerated electrons lowering the photocurrent the device can produce. Significant headway in this field could be made if processes were developed which allowed for a wide array of MOF structures to be grown via layer-by-layer growth or other means such as chemical vapor deposition.

In closing, MOFSCs present a unique avenue to the development of new state-of-the-art photovoltaics. The ability to fix chromophores into MOF backbones provides several distinct advantages over dye adsorption onto a nanostructured semiconductor electrode. These advantages include the prevention of dye aggregation and the ability to incorporate multiple chromophores, through variation of the MOF linker during synthesis, with various functionalities and absorption properties into the framework. Despite the challenges that MOFs face as sensitizers, they represent a novel molecular scaffold due to their unmatched synthetic tunability. The number of preliminary experimental results has increased dramatically in the last 5 years, with over one-hundred twenty independent studies exploring MOFs as either photosensitizers directly in MOFSCs, photoconductors, photodetectors, or as an additional component of more traditional DSSCs being published [25, 33, 42]. Compared to only five studies between the years of 2000–2012, this field is rapidly growing and expanding every year. It is feasible then to presume that the development optimization of new MOF materials for light harvesting applications will lead to MOFSCs emerging as one of the most promising candidates in the field of molecular photovoltaics.

Acknowledgments The authors wish to thank the US Department of Energy, Office of Basic Energy Sciences for funding under Award Number DE-SC0012445.

References

1. D.Y. Ahn et al., Novel solid-state solar cell based on hole-conducting MOF-sensitizer demonstrating power conversion efficiency of 21% ACS. Appl. Mater. Interfaces **9**, 12930–12935 (2017). https://doi.org/10.1021/acsami.7b03487
2. S.R. Ahrenholtz, C.C. Epley, A.J. Morris, Solvothermal preparation of an electrocatalytic metalloporphyrin MOF thin film and its redox hopping charge-transfer mechanism. J. Am. Chem. Soc. **136**, 2464–2472 (2014). https://doi.org/10.1021/ja410684q
3. M. Alvaro, E. Carbonell, B. Ferrer, F.X. Llabrés i Xamena, H. Garcia, Semiconductor behavior of a metal-organic framework (MOF). Chem. Eur. J. **13**, 5106–5112 (2007). https://doi.org/10.1002/chem.200601003
4. A.J. Bard, L.R. Faulkner, *Electrochemical Methods: Fundamentals and Applications* (Wiley, Hoboken, 2007)
5. G. Boschloo, A. Hagfeldt, Characteristics of the iodide/triiodide redox mediator in dye-sensitized solar. Cells Acc. Chem. Res. **42**, 1819–1826 (2009). https://doi.org/10.1021/ar900138m

6. A.M. Brun, A. Harriman, Energy- and electron-transfer processes involving palladium porphyrins bound to DNA. J. Am. Chem. Soc. **116**, 10383–10393 (1994). https://doi.org/10.1021/ja00102a004
7. P. Celis-Salazar, S. Ahrenholtz, A. Morris, Structural insight into redox hopping electron transport metal-organic frameworks. Am. Chem. Soc., INOR-244 (2016)
8. C.E.D. Chidsey, C.R. Bertozzi, T.M. Putvinski, A.M. Mujsce, Coadsorption of ferrocene-terminated and unsubstituted alkanethiols on gold: electroactive self-assembled monolayers. J. Am. Chem. Soc. **112**, 4301–4306 (1990). https://doi.org/10.1021/ja00167a028
9. M. Dan-Hardi, C. Serre, T. Frot, L. Rozes, G. Maurin, C. Sanchez, G. Férey, A new photoactive crystalline highly porous titanium(IV) dicarboxylate. J. Am. Chem. Soc. **131**, 10857–10859 (2009). https://doi.org/10.1021/ja903726m
10. M. de Miguel, F. Ragon, T. Devic, C. Serre, P. Horcajada, H. García, Evidence of photoinduced charge separation in the metal-organic framework MIL-125(Ti)-NH_2. ChemPhysChem **13**, 3651–3654 (2012). https://doi.org/10.1002/cphc.201200411
11. S. Goswami, M. Chen, M.R. Wasielewski, O.K. Farha, J.T. Hupp, Boosting transport distances for molecular excitons within photoexcited metal-organic framework films. ACS Appl. Mater. Interfaces **10**, 34409–34417 (2018). https://doi.org/10.1021/acsami.8b14977
12. S. Goswami, L. Ma, A.B..F. Martinson, M.R. Wasielewski, O.K. Farha, J.T. Hupp, Toward metal–organic framework-based solar cells: enhancing directional exciton transport by collapsing three-dimensional film structures. ACS Appl. Mater. Interfaces **8**, 30863–30870 (2016). https://doi.org/10.1021/acsami.6b08552
13. B.A. Gregg, M.E. Kose, Reversible switching between molecular and charge transfer phases in a liquid crystalline organic semiconductor. Chem. Mater. **20**, 5235–5239 (2008). https://doi.org/10.1021/cm800813h
14. T.G. Grissom, C.H. Sharp, P.M. Usov, D. Troya, A.J. Morris, J.R. Morris, Benzene, toluene, and xylene transport through UiO-66: diffusion rates, energetics, and the role of hydrogen bonding. J. Phys. Chem. C **122**, 16060–16069 (2018). https://doi.org/10.1021/acs.jpcc.8b03356
15. I. Hod et al., Bias-switchable permselectivity and redox catalytic activity of a ferrocene-functionalized, thin-film metal-organic framework compound. J. Phys. Chem. Lett. **6**, 586–591 (2015). https://doi.org/10.1021/acs.jpclett.5b00019
16. I. Hod, O.K. Farha, J.T. Hupp, Modulating the rate of charge transport in a metal-organic framework thin film using host: guest chemistry. Chem. Commun. **52**, 1705–1708 (2016). https://doi.org/10.1039/C5CC09695B
17. Y.-Q. Hu et al., Direct observation of confined $I^-\cdots I_2\cdots I^-$ interactions in a metal-organic framework: iodine capture and sensing. Chem. Eur. J. **23**, 8409–8413 (2017). https://doi.org/10.1002/chem.201702087
18. N. Ikeda, A. Yoshimura, M. Tsushima, T. Ohno, Hopping and annihilation of ^{3}MLCT in the crystalline solid of $[Ru(bpy)_3]X_2$ ($X = Cl^-$, ClO_4^- and PF_6^-). Chem. A Eur. J. **104**, 6158–6164 (2000). https://doi.org/10.1021/jp0002188
19. F.B. Kaufman, E.M. Engler, Solid-state spectroelectrochemistry of crosslinked donor bound polymer films. J. Am. Chem. Soc. **101**, 547–549 (1979). https://doi.org/10.1021/ja00497a009
20. C.A. Kent, D. Liu, T.J. Meyer, W. Lin, Amplified luminescence quenching of phosphorescent metal-organic frameworks. J. Am. Chem. Soc. **134**, 3991–3994 (2012). https://doi.org/10.1021/ja211271m
21. Y. Kobayashi, B. Jacobs, M.D. Allendorf, J.R. Long, Conductivity, doping, and redox chemistry of a microporous dithiolene-based metal-organic framework. Chem. Mater. **22**, 4120–4122 (2010). https://doi.org/10.1021/cm101238m
22. C.Y. Lee, O.K. Farha, B.J. Hong, A.A. Sarjeant, S.T. Nguyen, J.T. Hupp, Light-harvesting metal-organic frameworks (MOFs): efficient strut-to-strut energy transfer in bodipy and porphyrin-based MOFs. J. Am. Chem. Soc. **133**, 15858–15861 (2011). https://doi.org/10.1021/ja206029a
23. D.Y. Lee et al., Layer-by-layer deposition and photovoltaic property of Ru-based metal-organic frameworks. RSC Adv. **4**, 12037–12042 (2014a). https://doi.org/10.1039/C4RA00397G

24. D.Y. Lee, D.V. Shinde, S.J. Yoon, K.N. Cho, W. Lee, N.K. Shrestha, S.-H. Han, Cu-based metal-organic frameworks for photovoltaic application. J. Phys. Chem. C **118**, 16328–16334 (2014b). https://doi.org/10.1021/jp4079663
25. Y. Li, C. Chen, X. Sun, J. Dou, M. Wei, Metal-organic frameworks at interfaces in dye-sensitized solar cells. ChemSusChem **7**, 2469–2472 (2014). https://doi.org/10.1002/cssc.201402143
26. S. Lin, P.M. Usov, A.J. Morris, The role of redox hopping in metal-organic framework electrocatalysis. Chem. Commun. **54**, 6965–6974 (2018). https://doi.org/10.1039/C8CC01664J
27. W. Lu et al., Tuning the structure and function of metal-organic frameworks via linker design. Chem. Soc. Rev. **43**, 5561–5593 (2014). https://doi.org/10.1039/C4CS00003J
28. W.A. Maza, S.R. Ahrenholtz, C.C. Epley, C.S. Day, A.J. Morris, Solvothermal growth and photophysical characterization of a ruthenium(II) tris(2,2′-bipyridine)-doped zirconium UiO-67 metal-organic framework thin-film. J. Phys. Chem. C **118**, 14200–14210 (2014). https://doi.org/10.1021/jp5034195
29. W.A. Maza, A.J. Haring, S.R. Ahrenholtz, C.C. Epley, S.Y. Lin, A.J. Morris, Ruthenium(ii)-polypyridyl zirconium(iv) metal-organic frameworks as a new class of sensitized solar cells. Chem. Sci. **7**, 719–727 (2016). https://doi.org/10.1039/C5SC01565K
30. W.A. Maza, A.J. Morris, Photophysical characterization of a ruthenium(II) tris(2,2′-bipyridine)-doped zirconium UiO-67 metal-organic framework. J. Phys. Chem. C **118**, 8803–8817 (2014). https://doi.org/10.1021/jp501140r
31. B. O'Regan, M. Grätzel, A low-cost, high-efficiency solar cell based on dye-sensitized colloidal TiO_2 films. Nature **353**, 737 (1991). https://doi.org/10.1038/353737a0
32. P.J. Peerce, A.J. Bard, Polymer films on electrodes: part III. A digital simulation model for cyclic voltammetry of electroactive polymer film and electrochemistry of poly(vinyl ferrocene) on platinum. J. Electroanal. Chem. Interfacial Electrochem. **114**, 89–115 (1980). https://doi.org/10.1016/S0022-0728(80)80438-4
33. I.R. Perera, C.V. Hettiarachchi, R.J.K.U. Ranatunga, Metal-organic frameworks in dye-sensitized solar cells, in *Advances in Solar Energy Research*, ed. by H. Tyagi, A. K. Agarwal, P. R. Chakraborty, S. Powar, (Springer Singapore, Singapore, 2019), pp. 175–219. https://doi.org/10.1007/978-981-13-3302-6_7
34. P.G. Pickup, R.W. Murray, Redox conduction in mixed-valent polymers. J. Am. Chem. Soc. **105**, 4510–4514 (1983). https://doi.org/10.1021/ja00352a002
35. J.M. Rowe, J. Zhu, E.M. Soderstrom, W. Xu, A. Yakovenko, A.J. Morris, Sensitized photon upconversion in anthracene-based zirconium metal-organic frameworks. Chem. Commun. **54**, 7798–7801 (2018). https://doi.org/10.1039/C8CC01893F
36. D.T. Scholes, S.A. Hawks, P.Y. Yee, H. Wu, J.R. Lindemuth, S.H. Tolbert, B.J. Schwartz, Overcoming film quality issues for conjugated polymers doped with F_4TCNQ by solution sequential processing: hall effect, structural, and optical measurements. J. Phys. Chem. Lett. **6**, 4786–4793 (2015). https://doi.org/10.1021/acs.jpclett.5b02332
37. C.H. Sharp, J. Abelard, A.M. Plonka, W. Guo, C.L. Hill, J.R. Morris, Alkane–OH hydrogen bond formation and diffusion energetics of n-butane within UiO-66. J. Phys. Chem. C **121**, 8902–8906 (2017). https://doi.org/10.1021/acs.jpcc.7b01351
38. O. Shekhah et al., MOF-on-MOF heteroepitaxy: perfectly oriented $[Zn_2(ndc)_2(dabco)]_n$ grown on $[Cu_2(ndc)_2(dabco)]_n$ thin films. Dalton Trans. **40**, 4954–4958 (2011). https://doi.org/10.1039/C0DT01818J
39. K. Shigehara, N. Oyama, F.C. Anson, Electrochemical responses of electrodes coated with redox polymers. Evidence for control of charge-transfer rates across polymeric layers by electron exchange between incorporated redox sites. J. Am. Chem. Soc. **103**, 2552–2558 (1981). https://doi.org/10.1021/ja00400a011
40. C.G. Silva, A. Corma, H. García, Metal-organic frameworks as semiconductors. J. Mater. Chem. **20**, 3141–3156 (2010). https://doi.org/10.1039/B924937K
41. E.D. Spoerke et al., MOF-sensitized solar cells enabled by a pillared porphyrin framework. J. Phys. Chem. C **121**, 4816–4824 (2017). https://doi.org/10.1021/acs.jpcc.6b11251

42. V. Stavila, A.A. Talin, M.D. Allendorf, MOF-based electronic and optoelectronic devices. Chem. Soc. Rev. **43**, 5994–6010 (2014). https://doi.org/10.1039/C4CS00096J
43. C. Wang, J.-L. Wang, W. Lin, Elucidating molecular iridium water oxidation catalysts using metal-organic frameworks: a comprehensive structural, catalytic, spectroscopic, and kinetic study. J. Am. Chem. Soc. **134**, 19895–19908 (2012). https://doi.org/10.1021/ja310074j
44. H.S. White, J. Leddy, A.J. Bard, Polymer films on electrodes. 8. Investigation of charge-transport mechanisms in Nafion polymer modified electrodes. J. Am. Chem. Soc. **104**, 4811–4817 (1982). https://doi.org/10.1021/ja00382a013
45. S. Yuan et al., Stable metal-organic frameworks: design, synthesis, and applications. Adv. Mater. **30**, 1704303 (2018). https://doi.org/10.1002/adma.201704303
46. M.-H. Zeng, Q.-X. Wang, Y.-X. Tan, S. Hu, H.-X. Zhao, L.-S. Long, M. Kurmoo, Rigid pillars and double walls in a porous metal-organic framework: single-crystal to single-crystal, controlled uptake, and release of iodine and electrical conductivity. J. Am. Chem. Soc. **132**, 2561–2563 (2010). https://doi.org/10.1021/ja908293n
47. H.-C. Zhou, J.R. Long, O.M. Yaghi, Introduction to metal-organic frameworks. Chem. Rev. **112**, 673–674 (2012). https://doi.org/10.1021/cr300014x
48. J. Zhu, S. Shaikh, N.J. Mayhall, A.J. Morris, Energy transfer in metal-organic frameworks, in *Elaboration and Applications of Metal-Organic Frameworks* (Singapore, World Scientific), (2017), pp. 581–654. https://doi.org/10.1142/9789813226739_0014
49. HA. Lopez, A. Dhakshinamoorthy, B. Ferrer, P. Atienzar, M. Alvaro, H. Garcia Photochemical Response of Commercial MOFs: Al2(BDC)3 and Its Use As Active Material in Photovoltaic Devices The Journal of Physical Chemistry C **115**, 22200–22206 (2011). https://doi.org/10.1021/jp206919m